Visible cathodoluminescence of 4 Å single-walled carbon nanotubes

Y. F. Mei,[a] G. G. Siu, Ricky K. Y. Fu, and Paul K Chu
Department of Physics and Materials Science, City University of Hong Kong, Tat Chee Avenue, Kowloon, Hong Kong, China

Z. M. Li
School of Physics, Peking University, Beijing 100871, China

J. P. Zhai, H. J. Liu, and Z. K. Tang[b]
Department of Physics, Hong Kong University of Science & Technology, Clear Water Bay, Kowloon, Hong Kong, China

C. W. Lai and H. C. Ong
Department of Physics, The Chinese University of Hong Kong, Shatin, Hong Kong, China

(Received 14 January 2005; accepted 20 September 2005; published online 16 November 2005)

We report on cathodoluminescence (CL) of monosized and well-aligned 4 Å single-walled carbon nanotubes in a zeolite template ($AlPO_4$-5 single crystal). The CL exhibits three emission bands centered at 1.87, 2.22, and 2.98 eV, which are assigned to three possible 4 Å tube structures (4,2), (5,0), and (3,3), respectively. The assignation is based on first-principles calculations, Raman scattering measurement, and CL behavior of various samples. The emission peak shift of the (5, 0) tube is explained by the transition mechanism being different from photoluminescence due to the excitation of electrons with high energy. © *2005 American Institute of Physics*.
[DOI: 10.1063/1.2133912]

The 0.4-nm carbon nanotube[1–8] as a unique member of single-walled carbon nanotubes (SWNTs) exhibiting more interesting electrical (superconductivity)[6] and optical[8,9] properties. Much effort is being made to understand their nature.[5,7] They are possible to produce in large quantities, and easy to manipulate in the form of macroscopic samples. Their electronic properties have been optically probed by optical absorption[8] and photoluminescence[9] (PL) with the help of band structure calculations. In this letter, we report on cathodoluminescence (CL) of the 0.4-nm SWNTs array in the nanochannels of $AlPO_4$-5 single crystals (AFI in zeolite terminology).[1,4,6,8–11] The high excitation energy of conventional CL makes it useful to study radiative processes in most semiconductors and insulators even with large band gaps such as diamond, ZnO, BN, GaN, etc.[12] In our experiments, strong visible CL is contributed by three possible 0.4-nm nanotube structures: zigzag (5,0), armchair (3,3), and chiral (4,2). Instead of optically exciting electrons in the valance band, CL in the visible region is generated by secondary electrons that can combine with holes to form electron-hole pairs. This makes CL particularly superior in detecting the curvature effect in zigzag carbon nanotubes, as will be discussed in this letter.

AFI is a type of nanoporous alumino-phosphate single crystal. Its framework is transparent from the near infrared to ultraviolet spectral range. The ultrasmall SWNTs are monodispersed in 1-nm-sized parallel channels of AFI. They thus can be produced in large quantities, and manipulated in the form of macroscopic samples. An as-grown AFI crystal without any treatment contains tripropylamine [$(CH_3CH_2CH_2)_3N$, TPA] in its one-dimensional channels, which is named "as grown." The 0.4-nm SWNTs are generated in the channels by thermal pyrolysis of TPA. The fabrication process has been reported elsewhere.[1,6] In our experiments, to monitor the formation process of the 0.4-nm SWNTs, the AFI crystals were uniformly heated in a vacuum of 10^{-3} mbar at various temperatures (from 200 to 600 °C), and two critical temperatures, 375 and 580 °C, were chosen to demonstrate our results. These two temperatures are chosen because (1) 375 °C is the starting temperature at which the TPA molecules are thermally carbonized, C–C bonds are formed, and noncarbon atoms (H and N) are released in the form of amine and hydrogen gas and (2) 580 °C is the temperature at which TPA molecules are completely transformed to carbon nanotubes. If AFI crystals are heated to 580 °C in an oxygen atmosphere instead of vacuum, TPA will be oxidized and evacuated from the channels, with "empty" AFI channels left. Here, the resulting AFI crystal is noted as "empty." Room temperature CL spectra were collected by an Oxford Instrument MonoCL system installed in a scanning electron microscope (SEM) and CL images were observed under the panchromatic mode. Raman scattering measurements were performed on our samples at room temperature using an excitation wavelength of 514.5 nm on the JY T64000 Micro-Raman system.

In order to rule out the possibility that the CL originates from the AFI framework or residual TPA molecules, we prepared four samples: (1) As-grown AFI crystal containing TPA; (2) AFI containing 0.4-nm SWNTs after thermal treatment at 375 °C in vacuum; (3) AFI containing 0.4-nm SWNTs after thermal treatment at 580 °C in vacuum; and (4) pure AFI crystal with empty channels. Figure 1(a) shows their CL spectra, in which, samples 1 and 4 are featureless, while strong visible luminescence is detected from sample 3. Sample 2 also emits luminescence with the same spectral profile but low intensity. Figure 1(b) is a typical SEM image

[a]Current address: Max-Planck-Institut für Festkörperforschung, Heisenbergstrasse 1, D-70569 Stuttgart, Germany; electronic mail: meiyongfeng@nju.org.cn,
[b]Author to whom correspondence should be addressed; electronic mail: phzktang@ust.hk

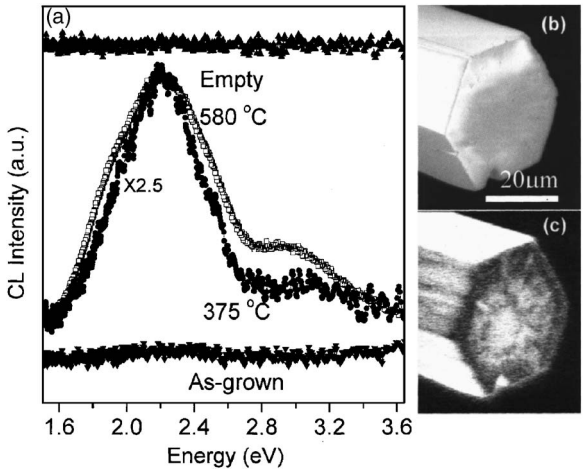

FIG. 1. (a) CL spectra of Sample (1) fresh AFI crystal containing TPA (named as as-grown), (2) AFI containing 4 Å SWNTs after thermal treatment at 375 °C in vacuum (375 °C), (3) AFI containing 4 Å SWNTs after thermal treatment at 580 °C in vacuum (580 °C), (4) empty AFI crystal without any CNTs or TPA (empty); (b) SEM image of AFI crystal containing 4 Å SWNT (Sample 3); and (c) its corresponding CL image.

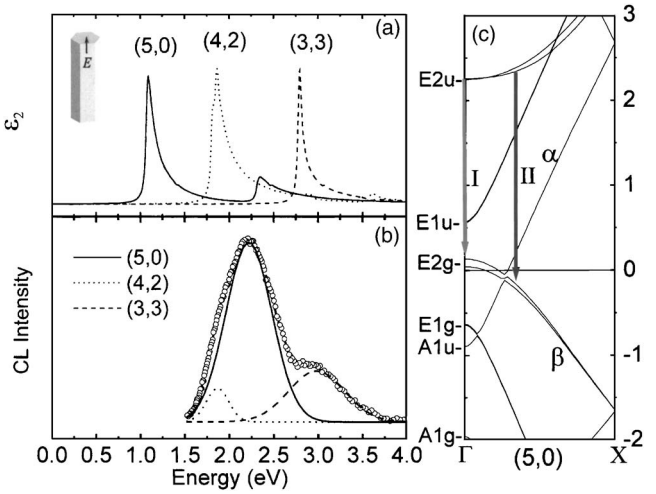

FIG. 3. (a) Imaginary part (2) of the dielectric function (parallel to the tube axis: its inset) for SWNT (4,2), (5,0), and (3,3); (b) CL spectra of Sample 3 by Gaussian deconvolution and its inset shows the CL intensity behavior of different SWNTs under electron bombardment; (c) calculated band structure for zigzag (5,0) SWNT and the Fermi level is at 0.

of the AFI containing 0.4-nm SWNT after thermal treatment at 580 °C (Sample 3), which shows a perfect hexagonal shape. The corresponding CL image is shown in Fig. 1(c).

Since CL is absent in the samples without any 0.4-nm SWNT in AFI channels, we can safely attribute the CL peaks to nanotubes structures. For confirmation, we acquired Raman spectra from the same set of samples 1, 2, and 3 as shown in Fig. 2(c). Based on previous assignment,[13–15] it can be seen that SWNTs start to grow in the AFI channels at 375 °C, as evidenced by the emergence of the *G* band (indicated by arrow). Thermal pyrolysis at a higher temperature of 580 °C leads to high quality and large quantity 0.4-nm SWNTs, as indicated by the strong radial breathing mode (labeled RBM) in the Raman spectra of Sample 3.[13] The CL images of samples 2 and 3 are also shown in Figs. 2(a) and 2(b). It can be observed that Sample 3 emits strong visible luminescence especially on its side faces, while that from Sample 2 is quite weak, indicating a low density of carbon nanotubes.

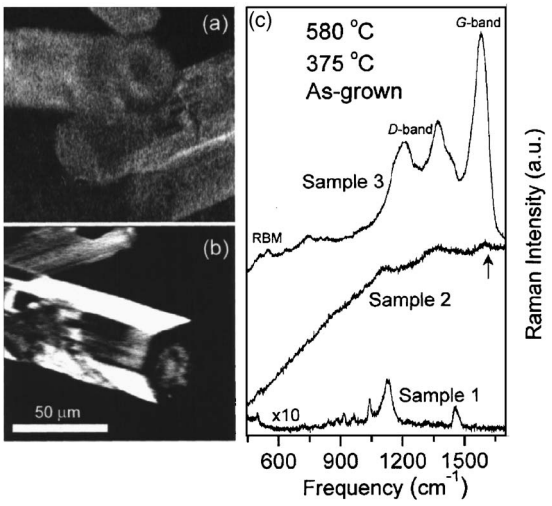

FIG. 2. CL images of (a) Sample 2 and (b) Sample 3; (c) Raman scattering spectra of Samples 1, 2, and 3.

Based on the information, we assign the CL peaks (in sample 3) to different types of the 0.4-nm tube structures. As shown in Fig. 3(b), the CL line shape can be fitted by three components centered at 1.87, 2.22, and 2.98 eV, respectively, based on Gaussian deconvolution. It should be noted that our CL spectra also exhibit broad emission bands, which are a little narrower than that of PL.[9] In PL, the width can likely be explained by the finite length distribution,[6] N-doped defect, or end states defects in the ultrasmall SWNTs.[9] Furthermore, the high excitation power may cause broadening of the CL spectra, which has been observed in quantum dots systems.[16] Hence, we consider that these effects may induce our broad CL emission. The understanding of the detailed and exact mechanism requires more careful experiments (at low temperature) and further theoretical calculation.

Figure 3(a) shows the imaginary part of the dielectric function (ε_2) calculated using an *ab initio* local density approximation (LDA) approach for the three types of 0.4-nm SWNTs in the case of light polarized parallel to the nanotube axis. The (5, 0), (4, 2), and (3, 3) tubes exhibit sharp peaks (due to nearest interband transitions) at 1.2 eV ($E_{1u} \rightarrow E_{1g}$), 1.89 eV ($E_{10u} \rightarrow E_{10g}$), and 2.8 eV ($E_u \rightarrow E_g$), respectively.[8] The (5,0) tube shows another weaker peak at 2.35 eV ($E_{2u} \rightarrow E_{2g}$) due to the second nearest interband transition. Comparing the calculated dielectric function with the measured CL spectra, we can attribute the CL bands at 1.87, 2.22, and 2.98 eV to the emission of the tubes (4, 2), (5, 0), and (3, 3), respectively. We could not carry out the measurement in the energy region lower than 1.5 eV, but it is reasonable to expect the existence of another CL peak due to the 1.2 eV transition of the (5, 0) tube. Figure 3 shows that the measured CL bands of the (4,2) tube at 1.87 eV agrees well with the calculated ε_2 spectra. The CL band of the (3,3) tube at 2.98 eV is, however, slightly higher than the transition energy of its calculated ε_2 spectrum due to the underestimation of band gap in the LDA calculation. For the same reason, the absorption band measured from the (3, 3) tube is also at a slightly higher energy than that predicted of the ε_2 peak.[8]

It is not straightforward to assign the CL peak at 2.22 eV to the (5, 0) SWNT. The deviation of the measured value

from the calculated transition energy (~2.35 eV) must arise from some physical mechanisms. The strong curvature effect in the zigzag (5, 0) tubes leads to the repulsion between antibonding σ bands and antibonding π bands, which pushes a π^* band (labeled α) down to cross the Fermi level. To balance the number of electronic states in the valance bands, two doubly degenerated bands (labeled β) emerge below the Fermi level. This effect is significant when optically probing the electronic properties of the (5, 0) tubes. The symmetry allows dipole transition between the E_{2u} and E_{2g} electronic bands and it turns out to be unlikely at the Γ point (indicated by the red arrow or I), since no electron can be excited. The transition becomes possible when the E_{2g} band falls below the Fermi level again, as indicated by the blue arrow or II. This transition (~2.35 eV) has been predicted by the first-principles calculation[11] and probed by the resonant Raman measurements.[18] However, this is not the case when probing the electronic band structure by CL. The secondary electrons generated by the cathodes are directly injected into the conduction bands. Through interband relaxation, electrons accumulate at the bottom of the E_{2u} and E_{1u} bands. Dipole allowed transition could occur between E_{2u} and E_{2g} at Γ point to give rise to the observed peak at 2.2 eV in the CL spectra. This effect can also qualitatively explain why the CL peak at 2.22 eV is stronger than two other ones. Since there are holes in the E_{2g} band ready to combine with immigrated electrons, the number of *e-h* pairs generated in the (5, 0) tubes can be large, while this is not the case for the (4, 2) and (3, 3) tubes.

Returning to Fig. 1, both the CL spectra of samples 2 and 3 are dominated by the emission of the (5, 0) tube. In the spectrum of sample 2, a much weaker CL emission is seen at 3.0 eV. In contrast, the emission band is clearly observed in the spectrum of sample 3. This fact indicates that the (5, 0) tubes are dominant in all the samples. The (3,3) tube seems to be hardly generated at low synthesis temperature (375 °C). This phenomenon can be explained in terms of the cohesive energy of the nanotubes. The cohesive energy (E) calculated based on the Tersoff potential for the three types of 0.4-nm SWNT decreases in the order of $E_{\text{armchair}} > E_{\text{Chiral}} > E_{\text{zigzag}}$.[17] The cohesive energy is highest for the (3,3) tube, and lowest for the (5, 0) tube. In other words, the (5, 0) tubes can be generated with a smaller energy than other two tube structures.

In conclusion, strong visible CL is contributed by three possible 4 Å nanotubes structures:, zigzag (5, 0), armchair (3, 3), and chiral (4, 2). The distinct luminescence has been analyzed based on first-principle calculations, Raman scattering measurement, and CL characteristics. Interesting changes in CL spectra are revealed in our ultrasmall SWNTs compared to their optical absorption and PL with the assistance of theoretical calculation.

The authors thank M. K. Tang and Dr. Amy X. Y. Lu for experimental assistance. This work was supported by Hong Kong Research Grants Council (RGC) Competitive Earmarked Research Grants (CERG) Nos. CityU 1137/03E, CityU 1120/04B, and HKUST 6057/02P.

[1] Z. K. Tang, H. D. Sun, J. Wang, J. Chen, and G. D. Li, Appl. Phys. Lett. **73**, 2287 (1998).
[2] L. F. Sun, S. S. Xie, W. Liu, W. Y. Zhou, Z. Q. Liu, D. S. Tang, G. Wang, and L. X. Qian, Nature (London) **403**, 384 (2000).
[3] L. C. Qin, X. L. Zhao, K. Hirahara, Y. Miyamoto, Y. Ando, and S. Iijima, Nature (London) **408**, 50 (2000).
[4] N. Wang, Z. K. Tang, G. D. Li, and J. S. Chen, Nature (London) **408**, 50 (2000).
[5] L. M. Peng, Z. L. Zhang, Z. Q. Xue, Q. D. Wu, Z. N. Gu, and D. G. Pettifor, Phys. Rev. Lett. **85**, 3249 (2000).
[6] Z. K. Tang, L. Zhang, N. Wang, X. X. Zhang, G. H. Wen, G. D. Li, J. N. Wang, C. T. Chan, and P. Sheng, Science **292**, 2462 (2001).
[7] X. Zhao, Y. Liu, S. Inoue, T. Suzuki, R. O. Jones, and Y. Ando, Phys. Rev. Lett. **92**, 125502 (2004).
[8] Z. M. Li, Z. K. Tang, H. J. Liu, N. Wang, C. T. Chan, R. Saito, S. Okada, D. Li, J. S. Chen, N. Nagasawa, and S. Tsuda, Phys. Rev. Lett. **87**, 127401 (2001).
[9] J. D. Guo, C. L. Yang, Z. M. Li, M. Bai, H. J. Liu, G. D. Li, E. G. Wang, C. T. Chan, Z. K. Tang, W. K. Ge, and X. D. Xiao, Phys. Rev. Lett. **93**, 017402 (2004).
[10] Z. M. Li, H. J. Liu, J. T. Ye, C. T. Chan, and Z. K. Tang. Appl. Phys. A: Mater. Sci. Process. **78**, 1211 (2004).
[11] H. J. Liu and C. T. Chan, Phys. Rev. B **66**, 115416 (2002).
[12] A. Gustafsson, M. E. Pistol, L. Montelius, and L. Samuelson, J. Appl. Phys. **84**, 1715 (1998).
[13] Z. M. Li, Z. K. Tang, G. G. Siu, and I. Bozovic, Appl. Phys. Lett. **84**, 4101 (2004).
[14] K. H. Schnabel, G. Finger, J. Kornatowski, E. Loffler, C. Peuker, and W. Pilz, Microporous Mater. **11**, 293 (1997).
[15] M. S. Dresselhaus, G. Dresselhaus, A. Jorio, A. G. Souza, and R. Saito, Carbon **40**, 2043 (2002).
[16] K. Akiba, N. Yamamoto, V. Grillo, A. Genseki, and Y. Watanabe, Phys. Rev. B **70**, 165322 (2004).
[17] S. Sawada and H. Hamada, Solid State Commun. **83**, 917 (1992).
[18] M. Hulman, H. Kuzmany, O. Dubay, G. Kresse, L. Li, and Z. K. Tang, J. Chem. Phys. **119**, 3384 (2003).